

62. R. W. Hendrix, *Proc. Natl. Acad. Sci. U.S.A.* **75**, 4779 (1978).
63. ———, *Cell* **94**, 147 (1998).
64. J. M. Valpuesta, J. J. Fernandez, J. M. Carazo, J. L. Carrascosa, *Structure* **7**, 289 (1999).
65. D. R. Thomas, D. G. Morgan, D. J. DeRosier, *Proc. Natl. Acad. Sci. U.S.A.* **96**, 10134 (1999).
66. F. Beuron *et al.*, *J. Struct. Biol.* **123**, 248 (1998).
67. D. A. Cherepanov, A. Y. Mulikdjanian, W. Junge, *FEBS Lett.* **449**, 1 (1999).
68. O. Pänke and B. Rumberg, *Biochim. Biophys. Acta* **1412**, 118 (1999).
69. T. Elston, H. Y. Wang, G. Oster, *Nature* **391**, 510 (1998).
70. R. A. Schemidt, J. Qu, J. R. Williams, W. S. A. Brusilow, *J. Bacteriol.* **180**, 3205 (1998).
71. R. A. Schemidt, D. K. W. Hsu, G. Deckers-Hebestreit, K. Altendorf, W. S. A. Brusilow, *Arch. Biochem. Biophys.* **323**, 423 (1995).
72. D. Turk, thesis, Technische Universität München, Munich, Germany (1992).
73. A. G. W. Leslie, *Joint CCP4 and ESF-EACMB Newsletter Protein Crystallography* (Daresbury Laboratory, Warrington, UK, 1992).

74. We thank R. Henderson for comments on the manuscript, S. Y. Peak-Chew and I. M. Fearnley for NH₂-terminal sequencing and HPLC analysis, and the staff of beamline ID02B at European Synchrotron Radiation Facility (ESRF), Grenoble, for help with data collection. D.S. was supported during part of this work by an European Molecular Biology Organization Fellowship. The coordinates of an unrefined C α model based on the bovine F₁ (1bmf) and the *E. coli* c (1a91) and ϵ (1aqt) coordinates have been deposited in the Protein Data Bank (accession code 1qo1).

27 September 1999; accepted 1 November 1999

REPORTS

First-Principles Determination of Elastic Anisotropy and Wave Velocities of MgO at Lower Mantle Conditions

B. B. Karki,¹ R. M. Wentzcovitch,¹ S. de Gironcoli,² S. Baroni²

The individual elastic constants of magnesium oxide (MgO) have been determined throughout Earth's lower mantle (LM) pressure-temperature regime with density functional perturbation theory. It is shown that temperature effects on seismic observables (density, velocities, and anisotropy) are monotonically suppressed with increasing pressure. Therefore, at realistic LM conditions, the isotropic wave velocities of MgO remain comparable to seismic velocities, as previously noticed in athermal high-pressure calculations. Also, the predicted strong pressure-induced anisotropy is preserved toward the bottom of the LM, so lattice-preferred orientations in MgO may contribute substantially to the observed seismic anisotropy in the D'' layer.

The last few years have seen rapid progress in our understanding of the behavior of the major mineral phases of Earth's mantle. Recent advances in theory and computation have made it possible to predict from first principles the structural and elastic properties of these materials throughout the entire pressure regime of the mantle (1). Experimental studies are now also possible over considerable ranges of pressure (P) and temperature (T) (2–5). However, the challenge of experimentally or theoretically determining the mineral properties at simultaneous P and T conditions of geophysical magnitudes is still enormous. Such studies will provide the basis for an improved analytical treatment of fundamental issues in Earth sciences, such as (i) constraining the mineralogy of the deep interior by directly comparing the seismic velocities (6) with predicted velocities for various mineral aggregates; (ii) describing Earth's thermal state by distinguishing thermal versus compositional effects on wave velocities; and (iii) understanding the sources of seismic anisotropies such as

those observed at D'' (7). It has been suggested that mantle flow and the accompanying stress field (in the vicinity of boundaries) could align crystalline axes along preferred directions and create anisotropic fabrics carrying the signature of the flow pattern (8).

The possibility of calculating with high accuracy and computational efficiency the entire vibrational spectrum of a crystal with the use of density functional perturbation theory (9) allows us to determine from first principles the crystal free energy, $F(V,T)$, from which we can extract all measurable thermodynamic quantities for the mineral, including the elastic moduli. Here we chose to start with the pressure and temperature dependence of the elastic constants of MgO (10), which exists as (Mg_{0.8}Fe_{0.2})O-magnesiowüstite in the lower mantle (LM) with 20 to 30% abundance according to a typical pyrolytic model (11). A previous first principles study of high-pressure (athermal) elasticity (12) showed that MgO is strongly anisotropic at D'' pressures (125 to 135 GPa) and its wave velocities are higher than seismic velocities throughout the LM pressure regime (23 to 135 GPa). Although T -induced effects at ambient P or so are known to be substantial and to counteract those of pressure

(4, 5), the effects at high P 's are unknown.

The results presented below were obtained within the quasi-harmonic approximation (QHA). It is a good approximation for MgO at ambient P up to ≈ 1000 K (13), as can be seen by comparing calculated and measured thermal expansivities, α (14) (see Fig. 1). The deviation of α from linearity at ambient P and high T 's is related to the inadequacy of the QHA and can be traced back to the behavior of the mode Grüneisen parameters with volume (15). The agreement with experiments at about 1800 K and 180 GPa (16), as well as the predicted linear behavior at high P 's and T 's, indicate that the QHA is valid at geophysically relevant conditions.

The adiabatic elastic constants (c_{11} , c_{12} , and c_{44}) were obtained as a function of P and T to 150 GPa and 3000 K, respectively, by calculating the free energies for the strained lattices (17). The predicted ambient values and their initial pressure (at 300 K) and temperature (at 0 GPa) dependencies agree with

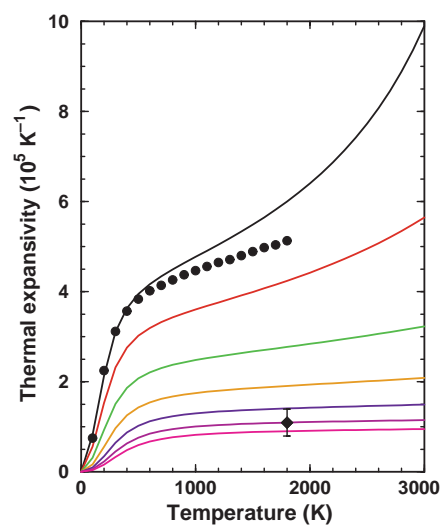


Fig. 1. Temperature dependence of thermal expansivity of MgO along several isobars at 0, 10, 30, 60, 100, 150, and 200 GPa (solid lines from top to bottom). The experimental data at zero pressure (14) are denoted by circles. The average value of α between 300 and ~ 3300 K at 169 to 196 GPa derived from shock-wave experiments (16) is denoted by the diamond.

¹Department of Chemical Engineering and Materials Science, Minnesota Supercomputing Institute, University of Minnesota, Minneapolis, MN 55455, USA.
²Scuola Internazionale Superiore di Studi Avanzati (SISSA), I-34014 Trieste, Italy.

REPORTS

measurements (3, 5) (Table 1 and Fig. 2). Our predicted cross P - T derivatives of c_{ij} 's are smaller (with opposite sign) than those obtained by experiments on MgO to 8 GPa and 1600 K (4). However, our results are consistent with earlier data to 0.8 GPa and 800 K (18) (Table 1) and potential-induced breathing (PIB) model calculations (19). Although uncertainties in the latest experiments are substantial (4), they are not such as to account for the observed disagreement, and, at this point, the reason for these discrepancies remains unclear. However, the cross deriva-

tive value of the bulk modulus (K_S) in (4) implies that K_S should start increasing with T at pressures higher than 8 GPa.

The pressure-induced change of sign in the single-crystal anisotropy, as expressed by $(2c_{44} + c_{12} - c_{11})/c_{11}$, is characteristic of MgO (3, 12, 20). Our results show that the strong P dependence of the anisotropy in MgO is preserved at high T (Fig. 2). Temperature effects counteract those of pressure and are monotonically suppressed as P increases. This result contrasts with the prediction based on extrapolations of experimental data obtained in a re-

duced P - T range (4). The latter suggests that T effects on anisotropy may actually increase with P .

MgO is likely to be the most anisotropic of the major LM phases at D'' conditions (21); therefore, lattice-preferred orientation (LPO) in MgO could produce anisotropies in shear waves with grazing incidence at the core-mantle boundary. Although LPO in MgO at LM conditions has not yet been studied, indirect inferences suggest that the {100} plane may be the dominant glide plane at D'' conditions (8). For a transversely isotropic aggregate, horizontal flow would then produce $V_{SH} > V_{SV}$ polarization anisotropy of ~35% in MgO (V is velocity, and SH and SV represent the horizontally and vertically polarized shear waves, respectively) that may be detectable in aggregates of pyrolytic composition. This is consistent with the $V_{SH} > V_{SV}$ anisotropy that was mostly observed in the D'' layer (in the circum- and central-Pacific regions) but not with the $V_{SV} > V_{SH}$ anisotropy that was also reported in the central-Pacific region (7). Although unknown LPOs in other major phases or shape-preferred orientations of lamellae mineral structures or melt pockets could also generate anisotropic structures, the elastic anisotropy of MgO predicted here is substantial and should be taken into account in attempts to explain the origin of seismic anisotropies in D''.

The density (ρ) and isotropic longitudinal

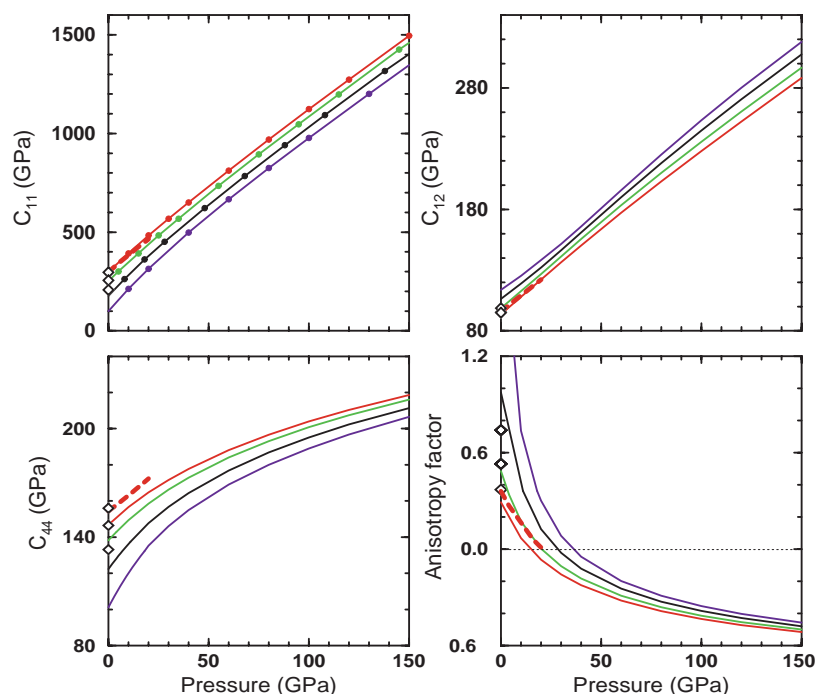


Fig. 2. Pressure dependence of calculated elastic constants (c_{ij} 's) and anisotropy factor of MgO along 300 (red), 1000 (green), 2000 (black), and 3000 (blue) K isotherms. Circles show pressures at which calculations were performed (same volume grid was used for all temperatures). Dashed red lines correspond to low-pressure (18.6 GPa) data at ambient temperature (3). The zero pressure data at 300, 1000, and 1800 K are indicated by diamonds (5).

Table 1. Adiabatic elastic moduli (M) of MgO and their pressure and temperature derivatives at ambient conditions. The modulus c_{110} corresponds to the longitudinal wave along [110] direction. The typical uncertainties in this type of calculation are expected to be within a few percent. The numbers in parentheses are experimental uncertainties.

| | c_{11} | c_{12} | c_{44} | c_{110} | K_S | G |
|--|-----------|----------|-------------|-----------|-----------|-----------|
| | | | This study | | | |
| M (GPa) | 300 | 94 | 147 | 344 | 162 | 128 |
| $\partial M/\partial P$ | 9.56 | 1.45 | 1.03 | 6.39 | 4.15 | 2.44 |
| $\partial M/\partial T$ | -0.0598 | 0.0089 | -0.0088 | -0.0343 | -0.0140 | -0.0216 |
| (GPa/K) | | | | | | |
| $\partial^2 M/\partial P \partial T$ | 0.56 | -0.06 | 0.20 | 0.45 | 0.14 | 0.44 |
| (10^{-3} 1/K) | | | | | | |
| | | | Experiments | | | |
| (3) M (GPa) | 297.9(15) | 95.8(10) | 154.4(20) | 351.3(22) | 163.2(10) | 130.2(10) |
| (3) $\partial M/\partial P$ | 9.05(20) | 1.34(15) | 0.84(20) | 6.04(37) | 4.0(1) | 2.4(1) |
| (5) $\partial M/\partial T$ | -0.0585 | 0.0075 | -0.0126 | -0.0381 | -0.0145 | -0.024 |
| (GPa/K) | | | | | | |
| (4) $\partial^2 M/\partial P \partial T$ | -1.3(4) | 5.1(24) | -0.2(3) | 1.7(7) | 3.0(15) | -1.8(10) |
| (10^{-3} 1/K) | | | | | | |
| (18) | 0.1(4) | 0.1(3) | 0.1(1) | 0.0(1) | 0.1(3) | 0.1(2) |

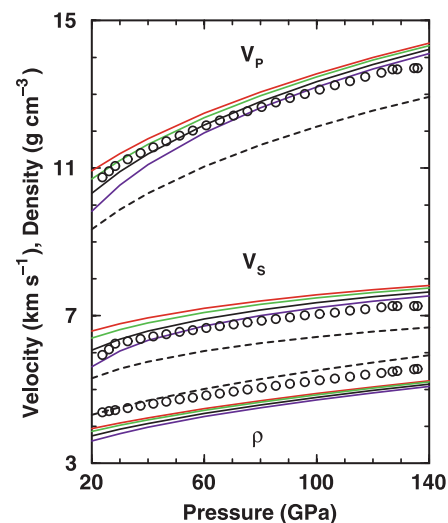


Fig. 3. Pressure dependence of density (ρ) and isotropic longitudinal (V_p) and shear (V_s) wave velocities of MgO at 300 (red), 1000 (green), 2000 (black), and 3000 (blue) K. Velocities are calculated from the bulk and shear moduli, K_S and G , as $V_p = \sqrt{(K_S + 4G/3)/\rho}$ and $V_s = \sqrt{G/\rho}$. Circles represent seismic observations of the lower mantle (6). Dashed lines represent magnesiowüstite with iron content (x) of 0.2 along the 2000 K isotherm. Although the effects of iron on K_S are negligible (22), the effects on ρ and G are large (22, 23), as can be estimated empirically with $\rho(x) = \rho(0)(1 + 0.76x)$ and $G(x) = G(0)(1 - 0.59x)$, where $\rho(0)$ and $G(0)$ are for the Mg end-member.

(V_p) and shear (V_s) wave velocities of MgO along several isotherms (Fig. 3) show that temperature effects decrease with pressure and the velocities of MgO remain comparable to the seismic velocities (6) in the upper half of the LM and are slightly larger in the lower half; however, the density of MgO is less than the bulk density of the LM. In the LM, the properties of MgO will be modified by the presence of iron. The wave velocities of magnesiowüstite should be lower than the seismic velocities of the LM, whereas their densities should be comparable (22–24).

The seismic parameter, $\nu = (\partial \ln V_s / \partial \ln V_p)_{P,T}$, is a measure of the relative lateral (isobaric) variations in V_s and V_p . Seismic tomography indicates that ν increases from ~ 1.7 from the top of the LM to a value exceeding 3 to the bottom (24). To understand whether such lateral heterogeneity can be of thermal origin requires a precise knowledge of ν for the component minerals at relevant conditions. High- T experiments at ambient pressures have yielded smaller values for ν (< 1.5) (5). Our calculated T dependence of the velocities constrains ν in MgO to vary from ~ 1.4 at the top to ~ 1.9 at the bottom of the LM. Earlier PIB calculations estimated $\nu \sim 2.5$ at the bottom of the LM (25). Our results suggest that unless ν is considerably larger in magnesiowüstite or silicate perovskite, the large lateral heterogeneity cannot be attributed to T effects alone if the mantle behaves as an elastic medium during the passage of seismic waves. However, the large seismic value of ν may be associated with anelastic effects that affect V_s more strongly than V_p at the low frequencies of seismic waves and high T 's (26).

tials were generated by the methods of U. von Barth and R. Car (unpublished data) for Mg and N. Troullier and J. L. Martins [*Phys. Rev. B* **43**, 1993 (1991)] for O. The plane wave cutoff was 90 rydbergs, and the Brillouin zone sampling included six special k points for equilibrium and up to 16 points for the strained lattices. Phonon dispersions were determined by diagonalization of the dynamical matrix obtained from linear electron-density response (9).

11. A. E. Ringwood, *Composition and Petrology of the Earth's Mantle* (McGraw-Hill, New York, 1975).
12. B. B. Karki et al., *Am. Mineral.* **82**, 51 (1997).
13. The calculated frequencies of Γ_{TO} , Γ_{LO} , X_{TA} , X_{LA} , X_{TO} , X_{LO} , X_{TA} , and X_{TO} phonons are 414, 710, 289, 433, 464, 555, 287, and 371 cm^{-1} , respectively, in agreement with the neutron scattering data of 408, 718, 299, 422, 443, 554, 288, and 369 cm^{-1} at ambient conditions [M. J. L. Sangster et al., *J. Phys. C* **3**, 1026 (1970)]. The equation of state parameters obtained from a fit of free energies to a fourth-order finite strain equation at ambient conditions are volume $V_0 = 18.81 \text{ \AA}^3$, isothermal bulk modulus $K_{TO} = 159 \text{ GPa}$, and its pressure derivatives $K_{TO}' = 4.30$ and $K_{TO}'' = -0.030 \text{ GPa}^{-1}$. They agree with the experimental values of $V_0 = 18.69 \text{ \AA}^3$, $K_{TO} = 160 \pm 2 \text{ GPa}$, and $K_{TO}' = 4.15$ determined under hydrostatic conditions (27). Our results at 1100 K, $V_0 = 19.44 \text{ \AA}^3$, $K_{TO} = 136 \text{ GPa}$, and $K_{TO}' = 4.48$ ($K_{TO}'' = -0.039 \text{ GPa}^{-1}$), are similar to the experimental values of $V_0 = 19.31 \text{ \AA}^3$, $K_{TO} = 135 \pm 3 \text{ GPa}$, and $K_{TO}' = 4.2$ (27). The calculated room temperature density varies from 5.45 to 5.65 g cm^{-3} at 169 to 196 GPa, compared with the shock-wave data of 5.50 to 5.70 g cm^{-3} (16).
14. Y. S. Touloukian, R. K. Kirdby, R. E. Taylor, T. Y. R. Lee, *Thermophysical Properties of Matter*, vol. 13 (IFI/Plenum, New York, 1977).
15. The mode Grüneisen parameters, defined as $\gamma_i = -d \ln \omega_i / d \ln V$, where ω_i is frequency, are nearly constant at small volumes and increase rapidly at large volumes.

The rapid increase in α at low P 's and high T 's is related to the rapid increase in γ_i 's at large equilibrium volumes.

16. T. S. Duffy and T. Ahrens, *Geophys. Res. Lett.* **20**, 1103 (1993).
17. We determined $c_s = (c_{11} - c_{12})/2$ and c_{44} for which isothermal and adiabatic values are identical by calculating free energies for strained (tetragonal and trigonal) configurations and relating them with the free energy expansion in terms of strains. The isothermal (K_T) and adiabatic (K_S) bulk moduli were determined from the equation of state parameters. Adiabatic (isothermal) c_{11} and c_{12} were then derived from c_s and K_S (K_T).
18. H. A. Spetzler, *J. Geophys. Res.* **75**, 2073 (1970).
19. D. G. Isaak, R. E. Cohen, M. E. Mehl, *J. Geophys. Res.* **95**, 7055 (1990).
20. T. S. Duffy, R. J. Hemley, H. K. Mao, *Phys. Rev. Lett.* **74**, 1371 (1995).
21. For instance, single-crystal polarization anisotropy in shear wave velocity at D' pressures is $\sim 55\%$ for MgO (12), compared with the anisotropy of ~ 13 , 7, 18, and 16% for MgSiO_3 perovskite, CaSiO_3 perovskite, SiO_2 , and CaO , respectively [B. B. Karki and L. Stixrude, *J. Geophys. Res.* **104**, 13025 (1999)].
22. T. S. Duffy and D. L. Anderson, *J. Geophys. Res.* **94**, 1895 (1989).
23. R. Jeanloz and A. B. Thompson, *Rev. Geophys.* **21**, 51 (1983).
24. A. M. Dziewonski and J. H. Woodhouse, *Science* **236**, 37 (1987); S. P. Grand, *J. Geophys. Res.* **99**, 11591 (1994).
25. D. G. Isaak, O. L. Anderson, R. E. Cohen, *Geophys. Res. Lett.* **19**, 741 (1992).
26. S. I. Karato, *Geophys. Res. Lett.* **20**, 1623 (1993).
27. Y. Fei, *Am. Mineral.* **84**, 272 (1999).
28. Supported by NSF grant EAR-9628042 and INFM of Italy. Computing facilities are provided by the Minnesota Supercomputing Institute. We thank S. Karato for useful discussions.

23 July 1999; accepted 20 October 1999

Core Rotational Dynamics and Geological Events

Marianne Greff-Lefftz¹ and Hilaire Legros²

A study of Earth's fluid core oscillations induced by lunar-solar tidal forces, together with tidal secular deceleration of Earth's axial rotation, shows that the rotational eigenfrequency of the fluid core and some solar tidal waves were in resonance around 3.0×10^9 , 1.8×10^9 , and 3×10^8 years ago. The associated viscomagnetic frictional power at the core boundaries may be converted into heat and would destabilize the D'' thermal layer, leading to the generation of deep-mantle plumes, and would also increase the temperature at the fluid core boundaries, perturbing the core dynamo process. Such phenomena could account for large-scale episodes of continental crust formation, the generation of flood basalts, and abrupt changes in geomagnetic reversal frequency.

The precession and nutations of Earth, as well as the secular variation of the length of day, are caused by lunar-solar gravitational torque (1, 2). In addition to this spatial motion, there is a tidally induced flow in the fluid core ($\vec{\omega}^c$) (3) [which can be observed with the use of superconducting gravimeters and very long baseline interferometry data] and a differential rotation

of the inner core with respect to the mantle ($\vec{\omega}^s$) (4, 5). These flows may resonate in the vicinity of the nearly diurnal period (6, 7), and their amplitudes depend on some geodynamical parameters such as the core flattening, the geodetic constant, and the tidal elastic Love numbers. Here, we calculate the epochs of resonance in the past as a function of Earth's rotation rate, and we investigate the associated dissipative power at the core-mantle boundary (CMB) and at the inner core boundary (ICB).

We use the classical Liouville equations (which describe the conservation of the angular momenta) in a form given by (5). This

References and Notes

1. R. M. Wentzcovitch, J. L. Martins, G. D. Price, *Phys. Rev. Lett.* **70**, 3947 (1993); B. B. Karki et al., *Am. Mineral.* **82**, 635 (1997).
2. G. Fiquet et al., *Phys. Earth Planet. Inter.* **105**, 21 (1998); S. Saxena et al., *Am. Mineral.* **84**, 226 (1999); J. D. Bass, in *Mineral Physics and Crystallography: A Handbook of Physical Constants*, T. Ahrens, Ed. (American Geophysical Union, Washington, DC, 1995), pp. 45–63; O. L. Anderson and G. D. Isaak, in *Mineral Physics and Crystallography: A Handbook of Physical Constants*, T. Ahrens, Ed. (American Geophysical Union, Washington, DC, 1995), pp. 64–97; C. S. Zha et al., *Earth Planet. Sci. Lett.* **159**, 25 (1998).
3. S. V. Sinogeikin and J. D. Bass, *Phys. Rev. B* **59**, 14141 (1999).
4. G. Chen, R. C. Liebermann, D. J. Weidner, *Science* **280**, 1913 (1998).
5. D. G. Isaak, O. L. Anderson, T. Goto, *Phys. Chem. Mineral.* **16**, 704 (1989).
6. A. M. Dziewonski and D. L. Anderson, *Phys. Earth Planet. Inter.* **25**, 297 (1981).
7. E. Matzel, M. K. Sen, S. P. Grand, *Geophys. Res. Lett.* **23**, 2417 (1996); E. J. Garnero and T. Lay, *J. Geophys. Res.* **102**, 8121 (1997); T. Lay, Q. Williams, E. J. Garnero, *Nature* **392**, 461 (1998).
8. S. Karato, *Earth Planets Space* **50**, 1019 (1998); *Pure Appl. Geophys.* **151**, 565 (1998).
9. S. Baroni, P. Giannozzi, A. Testa, *Phys. Rev. Lett.* **58**, 1861 (1987); P. Giannozzi et al., *Phys. Rev. B* **43**, 7231 (1991).
10. Calculations were carried out with the local density approximation [parameterization of J. P. Perdew and A. Zunger [*Phys. Rev. B* **23**, 5048 (1981)]]; Pseudopotentials

¹Department of Geomagnetism and Paleomagnetism, Institut de Physique du Globe de Paris, 4 place Jussieu, 75252 Paris 05, France. ²Ecole et Observatoire des Sciences de la Terre, 5 rue R. Descartes, 67084 Strasbourg, France.

First-Principles Determination of Elastic Anisotropy and Wave Velocities of MgO at Lower Mantle Conditions

B. B. Karki, R. M. Wentzcovitch, S. de Gironcoli and S. Baroni

Science **286** (5445), 1705-1707.
DOI: 10.1126/science.286.5445.1705

ARTICLE TOOLS

<http://science.sciencemag.org/content/286/5445/1705>

RELATED CONTENT

<file:/contentpending:yes>

REFERENCES

This article cites 29 articles, 6 of which you can access for free
<http://science.sciencemag.org/content/286/5445/1705#BIBL>

PERMISSIONS

<http://www.sciencemag.org/help/reprints-and-permissions>

Use of this article is subject to the [Terms of Service](#)